# IPM Traction Machine With Single Layer Non-Overlapping Concentrated Windings

Johannes J. Germishuizen and Maarten J. Kamper, *Senior Member, IEEE*

***Abstract*—In this paper, an interior permanent-magnet traction drive machine with single layer non-overlapping concentrated stator winding is analyzed. In the single layer winding design, the number of stator slots and a winding factor are specifically considered. Moreover, the effect of varying the coil pitch on the winding factor and torque pulsations is investigated. A new calculation method is proposed, whereby the constant torque and field-weakening speed characteristics of the machine drive can be predicted using torque and flux linkage functions. The measured and predicted field-weakening performance of a 150-kW direct traction drive machine is presented.**

***Index Terms*—Basic winding, design for manufacturability (DFM), non-overlapping concentrated winding, number of coils per pole and phase, 2-D functions.**

## NOMENCLATURE

| | |
|---|---|
| $b_t$ | Tooth width. |
| $b_s$ | Slot width. |
| $da_1$ | Stator outer diameter. |
| $di_1$ | Stator inner diameter. |
| $f$ | Frequency. |
| gcd | Greatest common divisor. |
| $I_1$ | Stator current. |
| $l_{Fe}$ | Stack length. |
| $m$ | Number of phases. |
| $N_s$ | Number of series turns per phase. |
| $p$ | Pole pair number. |
| $q$ | Number of slots per pole and phase. |
| $q_c$ | Number of coils per pole and phase. |
| $q_{cd}$ | Denominator of $q_c$. |
| $q_{cn}$ | Numerator of $q_c$. |
| $Q_b$ | Number of slots of the basic winding. |
| $Q_c$ | Number of coils. |
| $R_1$ | Stator per phase series resistance. |
| $t$ | $\gcd(Q_c, p)$. |
| $T$ | Torque. |
| $U_1$ | Line voltage. |
| $U_s$ | Phase voltage. |
| $y_p$ | Average coil pitch. |
| $y_d$ | Actual coil pitch. |
| $\alpha$ | Peripheral angle. |
| $\nu$ | Harmonic order. |
| $\omega$ | Polarity of a coil side. |
| $\xi$ | Winding factor. |
| $\psi$ | Flux linkage. |

Paper 2008-EMC-088.R1, presented at the 2007 Industry Applications Society Annual Meeting, New Orleans, LA, September 23–27, and approved for publication in the IEEE TRANSACTIONS ON INDUSTRY APPLICATIONS by the Electric Machines Committee of the IEEE Industry Applications Society. Manuscript submitted for review June 9, 2008 and released for publication February 18, 2009. Current version published July 17, 2009.

J. J. Germishuizen is with the Technology and Innovation Department, Loher GmbH, 94099 Ruhstorf, Germany (e-mail: johannes.germishuizen@loher.com).

M. J. Kamper is with the Department of Electrical and Electronic Engineering, Stellenbosch University, Stellenbosch 7602, South Africa (e-mail: kamper@sun.ac.za).

Color versions of one or more of the figures in this paper are available online at http://ieeexplore.ieee.org.

Digital Object Identifier 10.1109/TIA.2009.2023500

## I. INTRODUCTION

INDICATIONS are that the next generation of traction drives will be of the permanent-magnet synchronous machine (PMSM) direct drive type [1]. Various topologies are available when designing a drive system. The question is not whether to choose a PMSM but rather which topology, since it determines not only the drive performance but also the manufacturing. A machine with non-overlapping stator windings is well known in literature and, yet, not typical for rail traction. In this paper, the design aspects of an interior permanent magnet (IPM) rotor with non-overlapping concentrated windings in a railway traction drive application are investigated. At present, the state-of-the-art drive system of metro trains with underfloor traction equipment consists of a three-phase insulated-gate bipolar transistor converter feeding two or four induction traction motors in parallel. For the torque transmission to the wheel set, a gearbox is needed. There is a trend to replace the induction motor and gearbox with a direct drive system [2]. This reduces energy losses and investment and maintenance costs. Doing so improves efficiency and performance and results in lower life cycle costs [3].

The requirements of the motor used in a direct drive system are high torque-to-weight ratio and high efficiency. A motor type that fulfills this specification is the PMSM, since it has the highest torque density and efficiency [4]. Keeping **design for manufacturability** (DFM) in mind a suitable winding and rotor must be chosen. A PMSM topology with an IPM rotor is very attractive because of the following advantages.

1) The magnets are mechanically well protected.
2) Rectangular magnets can be used.
3) The rotor can be manufactured using magnetized magnets.
4) Simplified manufacturing compared to surface mount magnets and, thus, lower manufacturing costs.
5) The risk of demagnetization of the permanent magnets is smaller.

Similar advantages are reported in [5]. The influence of the winding on the design is described in the next section.

### A. Non-overlapping Concentrated Windings

At present, it is typical to use a double layer winding, form-wound coils, and insulation class 200 in a railway traction machine. A double layer winding leads to simpler end connections, and with form-wound coils, a high copper fill factor is possible. Although it is found that this winding type has a good performance [6], it is still quite expensive due to the high number of form-wound coils. A non-overlapping winding, on the other hand, has fewer coils than a distributed winding and simplifies the manufacturing. Different definitions of terminologies are in use for non-overlapping concentrated windings. The most common of these are as follows:

1) concentrated windings [7];
2) concentrated fractional pitch windings [8];
3) fractional slot wound [5];
4) fractional slot [9].

In German, this winding type is known as *Zahnspulen*, which, when translated, means tooth windings. Concentrated windings can be either overlapping or non-overlapping. The case of overlapping windings is referred to a coil that spans a pole pitch, whereas in the case of non-overlapping windings, it means that the coil is concentrated around a stator tooth. A fractional slot winding could be both. Overlapping fractional slot windings means that the coils of a phase are distributed over a variety of slots excluding one. Non-overlapping is always fractional. The authors prefer to classify a winding either as an overlapping or non-overlapping concentrated winding.

An alternative winding type for use in a traction machine is a non-overlapping concentrated winding, which could be either a single or double layer. Compared to overlapping winding, the non-overlapping has a shorter end-winding overhang, a simplified winding insulation, and a reduced number of stator coils [10], [11]. This implies that the active length can be increased, reduced copper in the end windings, an improved efficiency, and reduced manufacturing costs. The properties are summarized as follows:

1) **Non-overlapping double layer**. A non-overlapping double layer concentrated winding has a coil wound around each tooth, and the coil pitch is fixed. This usually leads to the use of round wire for which the insulation class 200 is not typical. The number of coils is equal to the number of slots. To reduce the cogging torque any further, the rotor must be skewed.
2) **Non-overlapping single layer**. Here, only every second stator tooth has a coil wound around it, and as a consequence, the coil pitch can be varied to improve the motor performance. This then leads to a stator design with alternating tooth widths similar to [12]. Form-wound coils and insulation class 200 can be used, and the coil number is half the slot number. For the same slot dimensions, a higher copper fill factor means less copper loss. It is not necessary to skew the rotor since the stator slot pitch can be varied to reduce the cogging torque.

In general, a disadvantage of non-overlapping concentrated windings, compared to distributed windings, is the higher magnetomotive force harmonics in the air gap [7]. Due to the higher order harmonics, the increased leakage inductance causes higher core losses and a need for a higher inverter rating. The field-weakening current in the constant power region will however be lower.

### B. Performance Analysis

For traction applications, it is necessary to design the motors to be efficient over the whole speed range. This requires a method to calculate the motor voltages, currents, and parameters accurately over a wide speed range. Due to motor nonlinearities and particularly the performance operation in the field-weakening range, a fast and precise method is required.

The use of finite-element (FE) transient solvers offers very accurate results, but the solution time required is insufficient for an all-day design environment. Analytical solutions, on the other hand, are fast, but due to motor nonlinearities, the accuracy is not high. In particular, in saturated machines, the motor parameters depend on the operating point [13], [14]. A compromise is to use a combination of the two methods.

In this paper, a method is presented to calculate the speed characteristic using torque and flux linkage functions, which are calculated by means of 2-D FE analysis. A similar method as used by [15] is used to take into account the effect of saturation and cross-magnetization.

## II. Traction Machine Design

In particular, fulfilling the class 200 insulation specification, the design and performance calculations in this paper are explained by means of 150-kW direct traction IPM machine with a non-overlapping concentrated winding. In this section, the necessary winding properties are explained, which are used to choose a slot number and the number of poles.

The winding is characterized by the number of stator slots per pole and per phase $q$. For an $m$-phase winding, this is expressed in terms of the number of stator slots $Q_s$ and the number of pole pairs $p$ as

$$q = \frac{Q_s}{2p\,m} \tag{1}$$

which holds for both single and double layer windings. A better way to characterize a winding is by defining the number of coils per pole and per phase $q_c$. In order to get the *basic winding*, which is the smallest repetitive part of the complete winding, $q_c$ should be represented as a reduced fraction, i.e.,

$$q_c = \frac{Q_c}{2p\,m} = \frac{q_{cn}}{q_{cd}} \qquad \begin{cases} Q_c = Q_s, & \text{double layer} \\ Q_c = \frac{1}{2}Q_s, & \text{single layer.} \end{cases} \tag{2}$$

The number of repetitions of the *basic winding* is given by the greatest common divisor $\gcd$ of $Q_c$ and $p$, i.e.,

$$t = \gcd(Q_c, p) \tag{3}$$

and the number of slots required for the *basic winding* will be

$$Q_b = \frac{Q_s}{t}. \tag{4}$$

The average coil pitch, in number of slots, is given by

$$y_p = \frac{Q_s}{2p} \tag{5}$$

which could be an integer or a fractional number. For a practical winding, the actual coil pitch must be an integer, i.e.,

$$y_d = \text{int}(y_p) \pm k \quad \begin{cases} k \in \mathbf{N} \\ y_p \geq 1. \end{cases} \tag{6}$$

From (1) and (2), in its reduced form, the *basic winding* parameters are summarized as follows.

1) The $Q_b$ slots represents $q_{cd}$ poles.
2) From the $Q_b$ slots, $q_{cn}$ must be assigned to a coil side of a phase. The return side of the coil is given by the coil pitch.

For double layer windings, a coil side is assigned to each slot in the bottom layer. The return side of the coil is given by the coil pitch $y_d$ in the top layer. In a single layer winding, the return side of the coil is in the same layer as that of the in-going coil side.

### A. Winding Factor

A winding factor could either be calculated without any knowledge of the winding layout [16] or it can be calculated on the basis of the winding layout as in [7] and [17]. The advantage of the latter is that the winding information to perform a FE analysis is available.

A general method to calculate the winding factor that incorporates both the pitch and distribution factors is used. An electromotive force phasor is assigned to each of the in- and outgoing coil sides of all the coils of a phase. The method also requires the mechanical angle $\alpha_i$ of the stator slot. The winding factor for a phase is then calculated as

$$\xi_p = \frac{3}{2Q_c}\left|\sum_{i=1}^{\frac{1}{3}Q_c} e^{j\phi_{i,p}} + e^{j(\phi_{i,p}-\phi_{\Delta,p})}\right|$$

$$e^{j\phi_{i,p}} = \text{in-going coil side}$$

$$e^{j(\phi_{i,p}-\phi_{\Delta,p})} = \text{outgoing coil side}$$

$$\phi_{i,p} = \left(\alpha_i p \frac{\pi}{180} + w_i\right)$$

$$\phi_{\Delta,p} = (k\alpha_p) y_d p \frac{\pi}{180}, \qquad 0 < k < y_p. \tag{7}$$

In (7), the summation is performed over $(1/3)Q_c$ coils per phase and is normalized by the number of coil sides per phase. $w_i$ is the polarity of a coil side. If the polarity is positive, $w_i = 0$, and for negative polarity, $w_i = \pi$. $\phi_\Delta$ means that the angle of the outgoing coil side can be calculated in terms of the angle of the in-going coil side, the coil pitch $y_d$, and the average angle per slot which is equal to

$$\alpha_p = \frac{2\pi}{Q_s}. \tag{8}$$

In a machine with $p$ pole pairs, the stator winding harmonic producing the magnetic field with $p$ pole pairs is called the *working harmonic*. This harmonic is always of the order $\nu = p$. The lowest winding harmonic is equal to the number of repetitions of the *basic winding*, as given in (3), i.e., $\nu_{\min} = t$. If $\nu_{\min} < p$, then the winding has a least one subharmonic.

In the case of a single layer non-overlapping concentrated winding, $k$ can vary between $0 < k < y_p$ and implies that the teeth around which the coils are wound and those between two adjacent coil sides can be different, i.e., an irregular distribution of the slots. This degree of freedom allows the designer to choose a coil pitch in such a way as to achieve an optimal winding factor and an improved design, i.e., maximum induced voltage. The tooth width of an overlapping double layer distributed and non-overlapping double layer concentrated winding usually is the same for all teeth and does not have this degree of freedom.

### B. Number of Stator Slots

The specifications for the stator slots are that it must be open, form-wound stator coils must be used, and, for the current application, [1] and [3], the stator inner diameter is 280 mm. Choosing the number of stator slots is bounded primarily by two factors.

1) For single layer non-overlapping windings, the number of stator slots must be a multiple of twice the number of phases, i.e., $Q_s \in \{6, 12, 18, 24, \ldots\}$.
2) DFM, which means that products are designed in such a way that they are easy to manufacture.

Since non-overlapping concentrated form-wound stator coils are used to achieve a high copper fill factor, the tooth width around which the coils are wound limits the radius of curvature. For a stator inner diameter of 280 mm, the possible slot number is in the range $24 \leq Q_s \leq 36$. For manufacturing, the best number of slots is chosen to be $Q_s = 30$. Skaar et al [16] proposed that the feasible region for the number of slots per pole and phase should be $(1/4) \leq q \leq (1/2)$. For manufacturability, the least number of poles is chosen, i.e., for $q = (1/2)$ $p = 10$. For this design, the average coil pitch is $y_p = 1.5$ slots. Using (6) and since a non-overlapping concentrated winding is required, $y_d = 1$. For analysis purposes, it is necessary to keep track of both the average coil pitch and the actual chosen coil pitch.

The FE model of the machine, which was optimized for minimum torque ripple and an improved winding factor, along with the flux lines with zero stator current, of the motor is shown in Fig. 1. Using (4), the *basic winding* has $Q_b = 6$ stator slots from which one slot has to be assigned to a coil side of phase A. The return coil side will be in the same layer and is determined by $y_d$. From the denominator of (2), the *basic winding* represents four rotor poles, and its parameters using (1)–(6) are summarized in Table I.

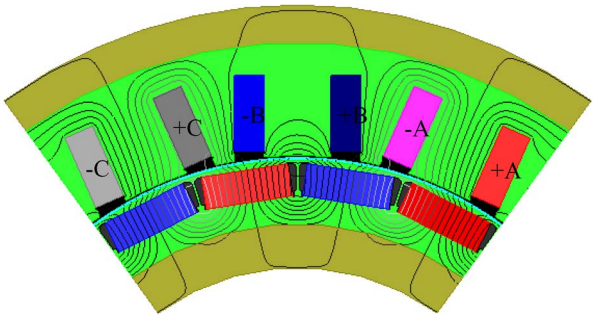


Fig. 1. FE model of a 20-pole 150-kW motor with single layer non-overlapping concentrated windings. The stator has an irregular distribution of the 30 stator slots. Notice that, because of the form-wound stator coils, the stator has open slots. This simplifies the manufacturing of the stator.

TABLE I
BASIC WINDING PARAMETERS FOR $Q_s = 30$ AND $p = 10$

| $Q_s$ | $Q_c$ | $q$ | $q_c$ | $q_{cn}$ | $q_{cd}$ | $t$ | $Q_b$ | $y_p$ | $y_d$ |
|---|---|---|---|---|---|---|---|---|---|
| 30 | 15 | $\frac{1}{2}$ | $\frac{1}{4}$ | 1 | 4 | 5 | 6 | $\frac{3}{2}$ | 1 |

TABLE II
WINDING FACTORS FOR THE MOTOR IN FIG. 1 USING (7)

| k | $\xi_5$ | $\xi_{10}$ | $\xi_{50}$ | $\xi_{70}$ |
|---|---|---|---|---|
| 1.00 | 0.50 | 0.87 | 0.87 | 0.87 |
| 1.05 | 0.52 | 0.89 | 0.71 | 0.99 |
| 1.10 | 0.54 | 0.91 | 0.50 | 0.98 |
| 1.15 | 0.57 | 0.93 | 0.25 | 0.83 |
| 1.20 | 0.59 | 0.95 | 0.00 | 0.59 |
| 1.25 | 0.61 | 0.96 | 0.26 | 0.26 |
| 1.30 | 0.63 | 0.97 | 0.50 | 0.10 |
| 1.50 | 0.71 | 1.00 | 1.00 | 1.00 |

The winding factors for different values of $k$ and $p$ are given in Table II. Setting $k = 1$, the winding factor is equal to 0.866. This is the same as in [7], [10], [16], and [18]. If $k = y_p$, it means that the coil spans a pole pitch and the winding factor is equal to one.

The winding factor calculation is verified by means of a FE analysis. Instead of calculating the air-gap field harmonics, the flux linkages, when moving the rotor, are evaluated for a certain magnet width. Noncommercial software that uses a special air-gap element in the FE method, [19] and [20], is used. There is no mesh in the air gap, which means that the rotor rotation is independent of the mesh and a suitable step size can be chosen that will simplify the discrete Fourier transformation of the flux linkages. The result of the fundamental flux linkage for different tooth widths is shown in Fig. 2. This verifies that, by increasing the tooth width, the fundamental winding factor can be increased.

### C. Torque Pulsation

There are three sources of torque ripple coming from the machine. They are cogging effect, distortion of the magnetic flux density distribution in the air gap, and the difference between permeances of the air gap in the $d$- and $q$-axes. Cogging torque in permanent magnet machines is caused by the interaction between a rotor magnetic flux and the variable permeance of the air gap due to stator slot geometry. For regular distributed stator slots, the number of cogging pulsations per rotor revolution is a

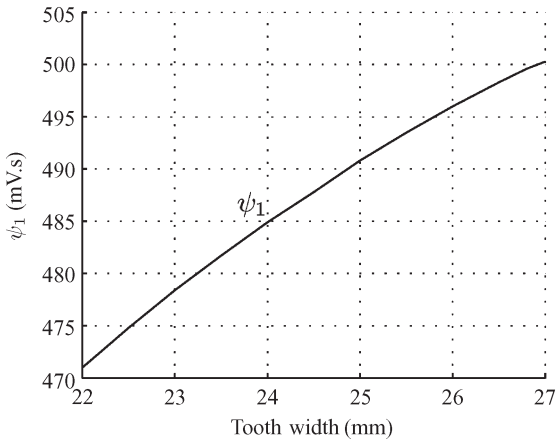


Fig. 2. No-load fundamental flux linkage versus tooth width.

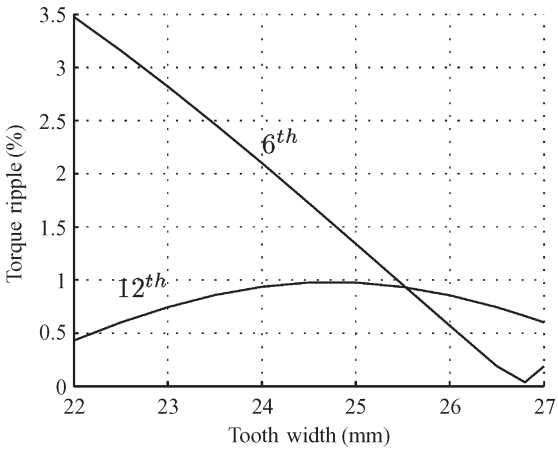


Fig. 3. Torque pulsation harmonics versus tooth width.

TABLE III
MAJOR MACHINE PARAMETERS

| Parameter | Description | Value |
|---|---|---|
| $da_1$ | stator outer diameter | 370 mm |
| $di_1$ | stator inner diameter | 280 mm |
| $b_t$ | tooth width | 26.6 mm |
| $b_s$ | slot width | 12.1 mm |
| $l_{Fe}$ | stack length | 786 mm |
| $N_s$ | series turns per phase | 45 |
| $R_1$ | per phase series resistance | 48.1 mΩ |

function of the least common multiple between $Q_s$ and $2p$ [10], i.e., lcm$(Q_s, 2p)$, and should be as high as possible.

Once the stator slot parameters are chosen, the stator tooth width or, equivalently, $k$ in (7) is varied to minimize the cogging torque. The torque as a function of the rotor position is calculated from air-gap element [19] and by rotating the rotor in the FE analysis. From a discrete Fourier transform of the torque, the rated torque and torque harmonics are calculated. Fig. 3 shows the torque harmonics as a percentage of the rated torque. It can be seen that the sixth torque harmonic can be reduced to zero if the tooth width is chosen to be 26.8 mm or, equivalently, $k = 1.20$. The major machine dimensions and parameters are given in Table III. The irregular distribution of the stator slots has another advantage, which reduces the no-load cogging torque.

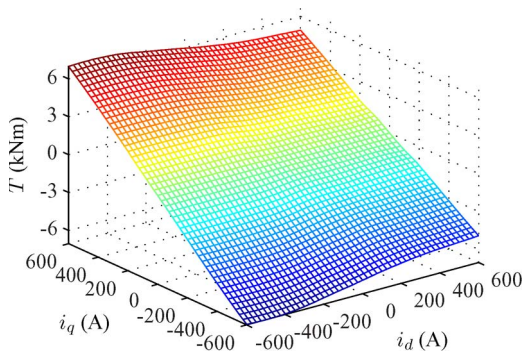


Fig. 4. Torque as a function of $i_d$ and $i_q$.

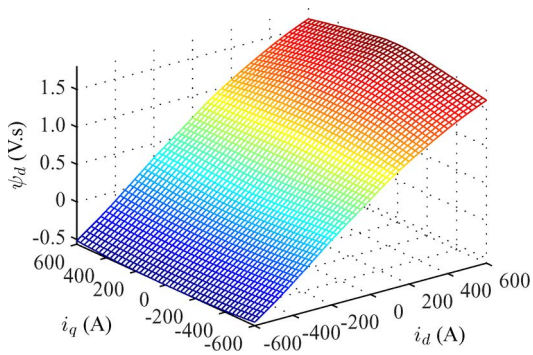


Fig. 5. $\psi_d$ as a function of $i_d$ and $i_q$.

## III. 2-D Flux and Torque Functions

In the performance calculations, the $dq$-model of electrical machines is used with the $dq$-reference frame fixed to the rotor that rotates at an electrical speed of $d\theta/dt$. The general equations that describe the motor voltages are

$$u_d = R_1 i_d + \frac{d\psi_d}{dt} - \frac{d\theta}{dt}\psi_q$$
$$u_q = R_1 i_q + \frac{d\psi_q}{dt} + \frac{d\theta}{dt}\psi_d \tag{9}$$

$$\left.\begin{aligned} u_d &= R_1 i_d - \omega\psi_q \\ u_q &= R_1 i_q + \omega\psi_d \end{aligned}\right\} \quad \frac{d\theta}{dt} = \omega. \tag{10}$$

From the power balance, the electromagnetic torque of the three-phase machine with $p$ pole pairs is given by

$$T = \frac{3}{2} p \left[\psi_m + (L_d - L_q) i_d\right] i_q \tag{11}$$

where $\psi_m$ is the flux linkage contribution of the permanent magnets.

For the frequency range under consideration, it is assumed that the flux linkages and torque are independent of frequency. This allows the calculation, by means of the FE method, of the flux linkages and torque for all possible combinations of the $d$- and $q$-axis currents. As a result, the motor can be described in terms of three 2-D functions, i.e., $T = f(i_d, i_q)$, $\psi_d = f(i_d, i_q)$, and $\psi_q = f(i_d, i_q)$, that include the saturation of the core. Once these functions are known for a specific design, it is possible, by means of 2-D interpolation routines, to easily calculate the motor performances over the whole speed range with high accuracy. The advantages of this method are as follows.

1) It is independent of any inductance calculations.
2) The flux linkages and torque can be scaled by the axial length and the number of series turns of the machine.
3) Saturation is automatically accounted for in the FE analysis.
4) It is independent of frequency.

Fig. 4 shows the 3-D representation of the torque function. Similar representations for the $d$- and $q$-axis flux linkages are shown in Figs. 5 and 6, respectively.

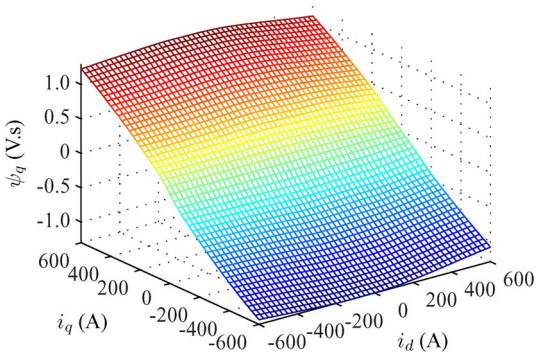


Fig. 6. $\psi_q$ as a function of $i_d$ and $i_q$.

### A. Torque Versus Frequency Characteristic

The torque versus frequency characteristic is characterized by two fixed regions, namely, the constant torque and constant power region. A field-weakening region is determined by the maximum allowable motor voltage and the number of series turns. Increasing the number of series turns will increase the voltage-to-frequency ratio. The previously described 2-D functions allow the torque versus speed characteristic to calculated without any knowledge of the inductances, which change considerably as a function of current excitation [21]. For a fixed axial length, the number of series turns is a design parameter. This allows the designer to evaluate the overall motor performance and particularly its performance in the field weakening range.

The following paragraph describes the method to obtain valid operating points over the whole speed range. For traction, a maximum torque per ampere control algorithm is often used. This, however, is only possible as long as the motor voltage is below the maximum allowable voltage. As soon as the maximum voltage has reached its limit, a different control scheme is necessary. Using the data $T = f(i_d, i_q)$, all the data points for a given torque command $T^*$

$$\{(i_{d1}, i_{q1}), (i_{d2}, i_{q2}), \ldots (i_{dn}, i_{qn})\} \in T = T^* \tag{12}$$

can be obtained by means of a 2-D interpolation function. Finding a valid operating point is summarized as follows.

1) Find the minimum stator current $I_{1,\min}$ from the set given in (12). Thus, with $i_d|_{T=T^*} = f(i_q)$, a 1-D interpolation is used to find $I_{1,\min}$.

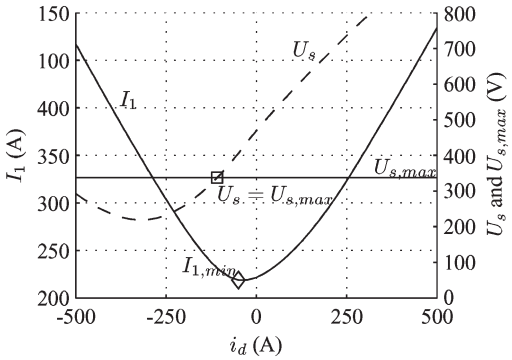


Fig. 7. Current locus for minimum current search.

2) With the pair $(i_d, i_q)|_{I_1=I_{\min}}$ known, get $\psi_d$ and $\psi_q$ from $\psi_d = f(i_d, i_q)$ and $\psi_q = f(i_d, i_q)$, respectively.
3) Get $u_d$ and $u_q$ from (9), and calculate the line voltage $U_1$.
4) Test if $U_1$ exceeds the maximum allowable voltage, i.e., $U_1 < U_{\max}$.
5) If $U_1 > U_{\max}$, decrease $i_d$ until $U_1 = U_{\max}$.

The stator current and line voltage are then calculated as

$$I_1 = \sqrt{\frac{i_d^2 + i_q^2}{2}}$$

$$U_1 = \sqrt{\frac{3\left(u_d^2 + u_q^2\right)}{2}}, \qquad U_1 < U_{\max} \tag{13}$$

respectively. The voltage constraint in (13) depends on the dc-bus voltage. Field weakening starts at the operating point where it is necessary to decrease $i_d$ or to make $i_d$ more negative. The current angle

$$\theta = \arctan\left(\frac{i_q}{i_d}\right) \tag{14}$$

needs then to be advanced to assure that the maximum voltage is not exceeded.

The operation of the motor in the field-weakening region is now graphically shown in Fig. 7 by making use of steps 1–5. For a given torque, a current locus is obtained from the 2-D functions, i.e., $I_1 = f(i_d)$. If the frequency at the operating point is known, the phase voltage for each point on the current locus can be calculated, i.e., $U_s = f(id)$. The minimum current is shown as $I_{\min}$. The voltage exceeds the maximum allowable voltage in this case, and this means that the current is increased in a negative direction toward the intersection of $U_s$ and $U_{s,\max}$ on the current locus. At this point, the voltage is equal to the maximum allowable voltage.

The flux linkages and current can be scaled by the number of series turns. Fig. 8 shows the voltage and current as functions of frequency for 45 and 75 of series turns per phase. This allows the designer to choose the number of series turns that best suits the dc bus and inverter rating. The chosen number of series turns determines the copper dimensions, and it is necessary to check the manufacturability of the coils. Setting the number of series turns to be equal to 45 means that the highest current in the constant torque region and field weakening starts at $f > 90$ Hz. Note the change in the voltage-to-frequency ratio

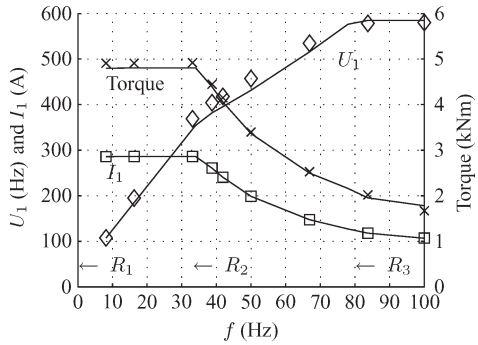


Fig. 8. Torque versus frequency characteristic for the number of series turns per phase equal to (dashed line) 45 and (solid line) 75. The machine with 45 series turns has thicker copper dimensions, and the slight increase in the current is partly caused by the skin effect.

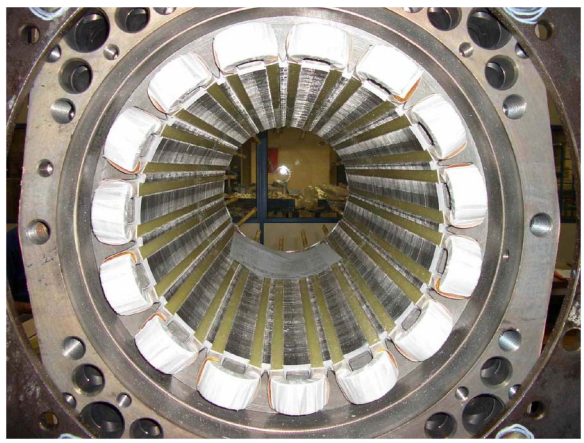

Fig. 9. Axial photograph of the stator having single layer non-overlapping concentrated coils. Note the short end windings and the low number of coils.

as soon as the motor is in the constant power region, i.e., the torque is proportional to the inverse of the frequency. When the number of series turns is increased to 75, the current in the constant torque region decreases, and the field weakening starts at $f = 40$ Hz. Thus, the higher the number of series turns per phase, the sooner the field weakening starts.

## IV. Prototype and Measured Results

An axial view into the bore of the stator is shown in Fig. 9. This clearly shows the short end windings and that there is no overlapping between the phases. The teeth width around which the coils are wounded is greater than those between two adjacent coils. For the 280-mm bore, the choice of slot number resulted in coils that could be manufactured without any difficulties.

The measurement setup of the 150-kW prototype is shown in Fig. 10. Since the machine was designed for a direct traction application, the axial length of the machine is limited by the distance between the railway tracks.

### A. No-Load Line Voltage

The no-load voltage is very sensitive to the remanent flux density $B_r$ of the magnets. It is almost always necessary to

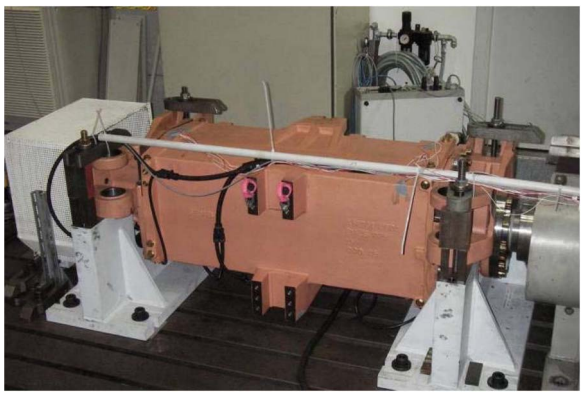

Fig. 10. Measurement setup for the 15-kW prototype shown in Fig. 1.

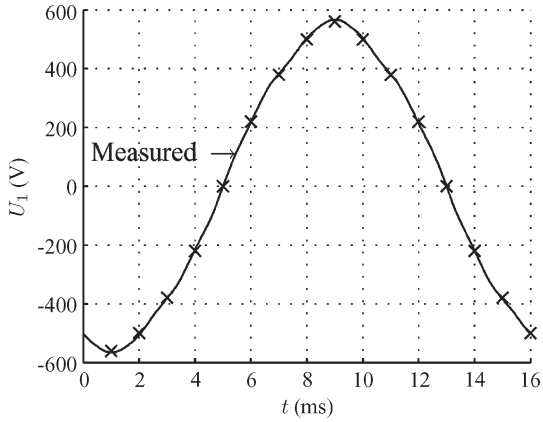


Fig. 11. Measured and calculated no-load line voltage at 62.5 Hz. The calculated no-load voltage corresponds excellently with those measured.

calibrate the FE model. The reason for this is that there is a difference between the minimum and typical values specified for $B_r$ in the data sheet. Depending on which value was used in the design, its value in the model should be changed to get the same no-load voltage as in the measured results. $B_r$ is also dependent on the quality of the manufacturer, which is usually unknown to the designer. The no-load voltage was measured at a room temperature of 30 °C or $\Delta T = 10$ K. In the FE model, it is necessary to set $\Delta T = 45$ K to get the same no-load voltage as was measured. The calculated induced voltage as a time function and that measured are shown in Fig. 11. Once the material properties in the model have been changed, the FE time-stepped results correspond excellently with those measured.

### B. Speed Characteristics

This paragraph gives the measured results in comparison with those calculated. For the comparison, the currents from the measurement were used to calculate the torque and voltages. The measured and calculated results for the torque, voltage, and current are shown in Fig. 12. A good comparison is obtained between calculated and measured results.

In the constant torque region $R_1$, the voltage-to-frequency ratio and the stator current $I_1$ are constant. Once the constant power region $R_2$ starts, the torque is proportional to the inverse of the frequency, and consequently, a lower voltage is

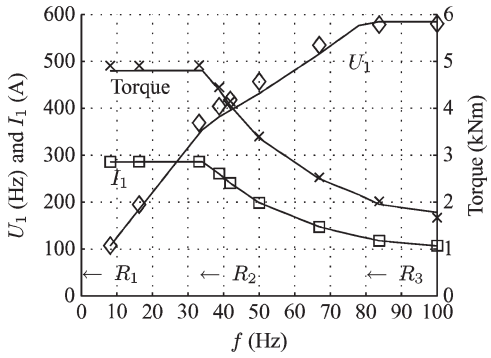


Fig. 12. Characteristic over the whole speed range. The field-weakening region starts at $R_3$.

required to obtain the maximum torque per ampere. This region is characterized by the lower voltage-to-frequency ratio. At speeds where the motor voltage exceeds the maximum voltage, field weakening is necessary. In this region, $R_3$, the voltage to frequency ratio is proportional to the inverse of the frequency.

## V. Conclusion

This paper has presented the design guidelines and methods for IPM machines with non-overlapping concentrated windings. Due to the high filling factor and slot pitch adjustment to reduce cogging torque, a single layer is chosen for the traction application. It has been shown that the adjustment of the coil pitch of the single layer winding can improve the winding factor and, thereby, the torque and harmonic-torque performance of the machine.

From 2-D FE analysis, the torque and flux linkages of the machine can be expressed as functions of $dq$-currents. Using these torque and flux functions, the performance of the IPM machine drive can be calculated fast and accurately for the whole speed range of the drive. This allows the designer to choose the best number of series turns that best suits the given dc-bus and inverter ratings easily. The validity of the proposed method is confirmed by measurements on a 150-kW railway traction drive machine.

## References

[1] A. Jöckel, L. Löwenstein, and M. Teichmann, "Syntegra—Innovative motor bogie technology with direct drives," *ZEVrail*, vol. 130, no. 9, pp. 368–379, 2006.

[2] A. Jöckel, L. Löwenstein, M. Teichmann, T. Hoffmann, and F. von Wangelin, "Syntegra—Innovativer prototyp einer naechsten triebfahrwerk-generation," *Elektr. Bahnen*, vol. 104, no. 8/9, pp. 360–362, 364–366, 368–369, 2006.

[3] J. Germishuizen, A. Jöckel, T. Hoffmann, M. Teichmann, L. Löwenstein, and F. von Wangelin, "Syntegra—Next generation traction drive system, total integration of traction, bogie and braking technology," in *Proc. SPEEDAM*, Taormina, Italy, May 2006, pp. 23–27.

[4] J. Gieras and I. Gieras, "Electric motors—The future," in *Proc. EPE-PEMC*, Kosice, Slovakia, Sep. 2000, vol. 1, pp. 12–18.

[5] P. Salminen, J. Mantere, J. Pyrhönen, and M. Niemelä, "Performance analysis of fractional slot wound PM-motors," in *Proc. ICEM*, Cracow, Poland, Sep. 2004.

[6] T. Koch and A. Binder, "Permanent magnet synchronous direct drive for high speed trains," in *Proc. ELECTROMOTION*, Bologna, Italy, Jun. 2001, pp. 287–292.

[7] F. Magnussen and C. Sadarangani, "Winding factors and joule losses of permanent magnet machines with concentrated windings," in *Proc. IEMDC*, Madison, WI, Jun. 2003, vol. 1, pp. 333–339.

[8] F. Magnussen, D. Svechkarenko, P. Thelin, and C. Sadarangani, "Analysis of a PM machine with concentrated fractional pitch windings," in *Proc. Nordic Workshop Power Ind. Electron.*, 2004.
[9] N. Bianchi and S. Bolognani, "Fractional-slot PM motors for electric power steering systems," *Int. J. Veh. Auton. Syst.*, vol. 2, no. 3/4, pp. 189–200, 2004.
[10] J. Cros and P. Viarouge, "Synthesis of high performance PM motors with concentrated windings," *IEEE Trans. Energy Convers.*, vol. 17, no. 2, pp. 248–253, Jun. 2002.
[11] G. Huth and K. Qian, "Permanentmagneterregte AC-servomotoren mit vereinfachten wicklungssystem," *ETG-Fachberichte*, vol. 96, pp. 15–21, 2004.
[12] T. Koch and A. Binder, "Permanent magnet machines with fractional slot winding for electric traction," in *Proc. ICEM*, Brugges, Belgium, Aug. 2002.
[13] M. A. Rahman and P. Zhou, "Analysis of brushless permanent magnet synchronous motors," *IEEE Trans. Ind. Electron.*, vol. 43, no. 2, pp. 256–267, Apr. 1996.
[14] K. Reichert, "A simplified approach to permanent magnet and reluctance motor characteristics determination by finite-element methods," in *Proc. ICEM*, Cracow, Poland, Sep. 2004.
[15] B. Stumberger, G. Stumberger, D. Dolinar, A. Hamler, and M. Trlep, "Evaluation of saturation and cross-magnetization effects in interior permanent-magnet synchronous motor," *IEEE Trans. Ind. Appl.*, vol. 39, no. 5, pp. 1264–1271, Sep./Oct. 2003.
[16] S. Skaar, O. Krovel, and R. Nilssen, "Distribution, coil-span and winding factors for PM machines with concentrated windings," in *Proc. ICEM*, 2006.
[17] K. Reichert, "PM-motors with concentrated, non overlapping windings, some characteristics," in *Proc. ICEM*, Cracow, Poland, Sep. 2004.
[18] F. Libert and J. Soulard, "Investigation on pole-slot combinations for permanent-magnet machines with concentrated windings," in *Proc. Int. Conf. Elect. Mach.*, 2004, pp. 530–535.
[19] A. Abdel-Razek, J. Coulomb, M. Feliachi, and J. Sabbonadiere, "The calculation of electromagnetic torque in saturated electric machines within combined numerical and analytical solutions in the field equations," *IEEE Trans. Magn.*, vol. MAG-17, no. 6, pp. 3250–3252, Nov. 1981.
[20] A. Abdel-Razek, J. Coulomb, M. Feliachi, and J. Sabonnadiere, "Conception of an airgap element for the dynamic analysis of the electromagnetic field in electric machines," *IEEE Trans. Magn.*, vol. MAG-18, no. 2, pp. 655–659, Mar. 1982.
[21] M. Bech, T. Frederiksen, and P. Sandholdt, "Accurate torque control of saturated interior permanent magnet synchronous motors in the field-weakening region," in *Conf Rec. IEEE IAS Annu. Meeting*, 2005, pp. 2526–2532.

**Johannes J. Germishuizen** received the M.Sc. (Eng.) and Ph.D. (Eng.) degrees from the University of Stellenbosch, Stellenbosch, South Africa, in 2000 and 2009, respectively.

In April 2000, he joined the Traction Motor Development Department, Siemens AG, Nürnberg, Germany, where he worked as a Design Engineer. Since March 2008, he has been with the Technology and Innovation Department, Loher GmbH, Ruhstorf, Germany. His research interests include the design of reluctance, permanent-magnet, and induction machine drives.

**Maarten J. Kamper** (SM'08) received the M.Sc. (Eng.) and Ph.D. (Eng.) degrees from the University of Stellenbosch, Stellenbosch, South Africa, in 1987 and 1996, respectively.

He has been a Member of the Academic Staff of the Department of Electrical and Electronic Engineering, University of Stellenbosch, since 1989, where he is currently a Professor of electrical machines and drives. His research interests include computer-aided design, and control of reluctance, permanent-magnet, and induction machine drives.

Prof. Kamper is a South African National Research Foundation Supported Scientist and a Registered Professional Engineer in South Africa.